Neuron
Article

GABAergic Lateral Interactions Tune the Early Stages of Visual Processing in *Drosophila*

Limor Freifeld,[1] Damon A. Clark,[2,6] Mark J. Schnitzer,[3,4,5] Mark A. Horowitz,[1] and Thomas R. Clandinin[2,*]
[1]Department of Electrical Engineering
[2]Department of Neurobiology
[3]Department of Biological Sciences
[4]Howard Hughes Medical Institute
[5]Department of Applied Physics
Stanford University, Stanford, CA 94305, USA
[6]Department of Molecular, Cellular, and Developmental Biology, Yale University, New Haven, CT 06520, USA
*Correspondence: trc@stanford.edu
http://dx.doi.org/10.1016/j.neuron.2013.04.024

SUMMARY

Early stages of visual processing must capture complex, dynamic inputs. While peripheral neurons often implement efficient encoding by exploiting natural stimulus statistics, downstream neurons are specialized to extract behaviorally relevant features. How do these specializations arise? We use two-photon imaging in *Drosophila* to characterize a first-order interneuron, L2, that provides input to a pathway specialized for detecting moving dark edges. GABAergic interactions, mediated in part presynaptically, create an antagonistic and anisotropic center-surround receptive field. This receptive field is spatiotemporally coupled, applying differential temporal processing to large and small dark objects, achieving significant specialization. GABAergic circuits also mediate OFF responses and balance these with responses to ON stimuli. Remarkably, the functional properties of L2 are strikingly similar to those of bipolar cells, yet emerge through different molecular and circuit mechanisms. Thus, evolution appears to have converged on a common strategy for processing visual information at the first synapse.

INTRODUCTION

The complexity of the visual world demands significant neural processing to extract behaviorally relevant information. What processing strategies enable peripheral visual circuits to capture and transform these inputs? Early visual processing neurons are tuned to maximize encoded information (Laughlin, 1981), while downstream neurons are specialized to encode specific features, such as motion, discarding irrelevant information (Masland, 2001; Borst et al., 2010; Gollisch and Meister, 2010). How these two competing objectives are balanced at intermediate processing steps is poorly understood. Here we address this question by examining the functional characteristics of a first-order interneuron that provides inputs to a specialized motion detection pathway in the *Drosophila* visual system.

Lateral inhibitory interactions among peripheral input channels constitute an essential part of neural processing across many sensory modalities in both vertebrates and invertebrates (Knudsen and Konishi, 1978; Brumberg et al., 1996; Dacey et al., 2000; Wilson and Laurent, 2005). In the visual system, lateral inhibition produces a variety of center-surround receptive field (RF) structures in many types of interneurons, including bipolar and ganglion cells in the vertebrate retina, as well as first-order interneurons in flies and other arthropods (Hartline et al., 1956; Werblin and Dowling, 1969; Kaneko, 1970; Dubs, 1982; Enroth-Cugell and Freeman, 1987; Dacey et al., 2000). Lateral inhibition enhances basic visual features such as edges and suppresses responses to spatially uniform intensity (Ratliff et al., 1963; Laughlin, 1994). Several theories derive ideal antagonistic center-surround organizations designed to reduce redundancy or maximize information transmission under constraints posed by input statistics and broad behavioral goals (Barlow, 1961; Srinivasan et al., 1982; Srinivasan, 1990; Atick, 1992; van Hateren, 1992; Olshausen and Field, 1996). However, it is unclear how input channels might satisfy efficient encoding goals while simultaneously enhancing features central to specific downstream computations.

The fly visual system provides a powerful model for examining how neural circuit mechanisms shape behavioral responses to visual motion (reviewed in Borst et al., 2010). R1–R6 photoreceptors relay local intensity signals to three lamina monopolar cells (LMCs), L1–L3, arranged in a retinotopic array (reviewed in Clandinin and Zipursky, 2002). Under bright illumination, LMCs transiently hyperpolarize to light increments, depolarize to decrements, and have antagonistic center surrounds (Järvilehto and Zettler, 1973; Laughlin and Hardie, 1978; Dubs, 1982; Laughlin et al., 1987; Laughlin and Osorio, 1989; van Hateren, 1992). Pharmacological and ultrastructural studies demonstrated that these cells receive inputs from additional circuit elements (Hardie, 1987; Meinertzhagen and O'Neil, 1991; Rivera-Alba et al., 2011). However, how this dense connectivity shapes the outputs of the lamina is unknown. Genetic manipulations have

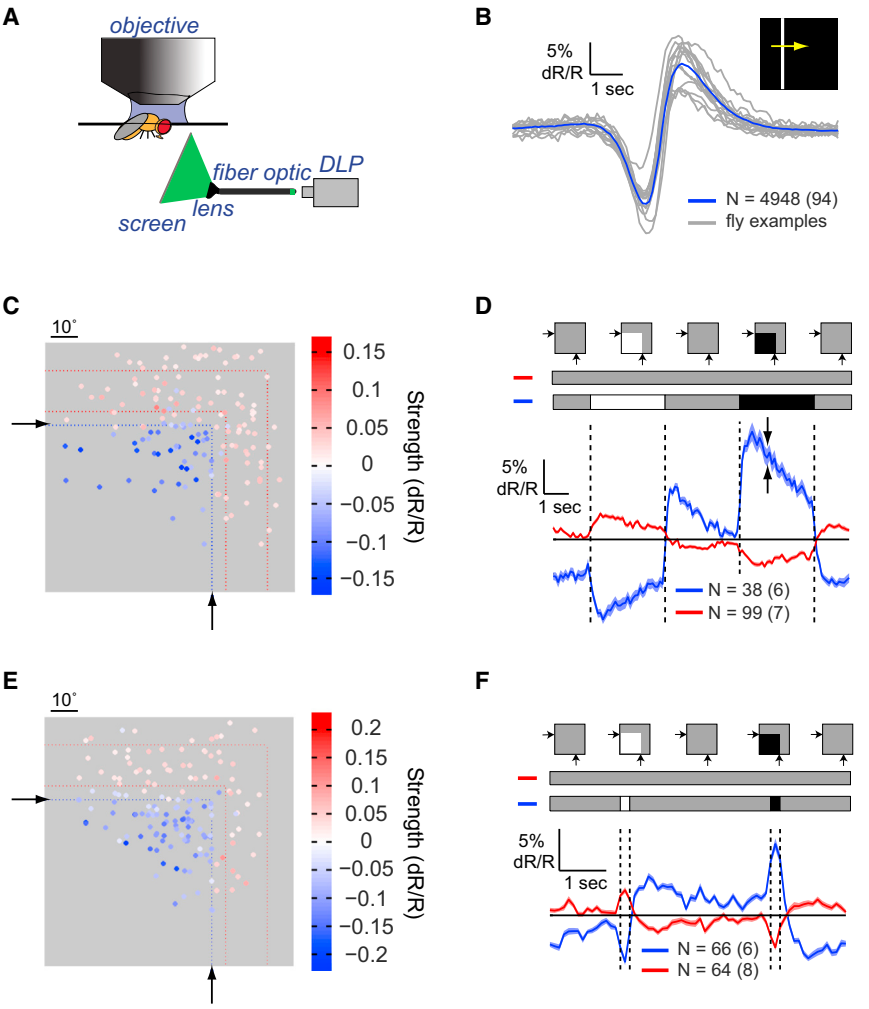

Figure 1. Lateral Inhibition Shapes L2 Cell Responses to Light

(A) Schematic illustration of the imaging set-up. DLP, digital light projector.

(B) Mean response of all L2 cells (blue) and average responses from a few example flies (gray) to a bright bar moving on a dark background. N denotes the number of cells, with the number of flies denoted parenthetically. Shading denotes ±1 SEM.

(C and D) The response of L2 cells to a partial field flash.

(C) Heat map of response strengths as a function of the RF center location on the screen, indicated by dots. Colors indicate the strength and sign of the corresponding cell response. Only cells with response strengths >0.025 or <−0.015 are presented. Black arrows and blue dotted lines denote the region of the screen where the flash was presented. Red dotted lines denote the region of the screen where surround responses in (D) were observed.

(D) Mean response of L2 cells to the flash presentation, separated by polarity and position. Blue, cells within the flash presentation region, which hyperpolarized to light; red, cells outside of the flash presentation region, which depolarized to light. Shading denotes ±1 SEM (highlighted by the two arrows). Top: schematic description of the stimulus, including the contrast inputs into each group of cells.

(E and F) Same as (C) and (D) for cells responding to a 200 ms flash presentation, including only cells with response strengths larger than a 0.02 threshold. See also Figure S1.

demonstrated that L2 cells provide inputs to a pathway specialized for detecting moving dark edges (Rister et al., 2007; Joesch et al., 2010; Clark et al., 2011). Most electrophysiological studies of LMCs did not distinguish individual cell types and did not observe functional properties in L2 cells related to this specialization (Laughlin and Osorio, 1989). However, one of two studies that examined calcium signals in L2 axon terminals reported that L2 predominantly transmitted information about light decrements (Reiff et al., 2010), while the other observed that L2 responded strongly to both increments and decrements (Clark et al., 2011). Thus, it remains unclear how the functional properties of L2 might contribute to the specialization of the downstream pathway. Here we examine the response properties of L2 using in vivo two-photon Ca^{2+} imaging, pharmacology, and genetics and relate these responses to downstream circuit specializations.

RESULTS

L2 Responses to Light Are Shaped by Antagonistic Lateral Inputs

To examine how activity in the axon terminals of L2 cells is shaped by different spatiotemporal patterns of light, we modified an existing apparatus for presenting visual stimuli during two-photon in vivo imaging in *Drosophila* (Figure 1A; Clark et al., 2011). A digital light projector displayed stimuli on an optical fiber bundle that was imaged onto a screen positioned in front of one eye. The ratiometric, FRET-based indicator TN-XXL (Clark et al., 2011; Mank et al., 2008; Reiff et al., 2010) was expressed in L2 cells, providing an optical report of changes in Ca^{2+} concentration. Light depolarizes *Drosophila* photoreceptors and hyperpolarizes LMCs via histamine-gated Cl^- channels (Hardie, 1987, 1989). Reflecting these changes in membrane voltage, L2 axon terminals displayed decreases and increases in intracellular Ca^{2+} concentration in response to light increments and decrements, respectively (Reiff et al., 2010; Clark et al., 2011). To relate stimulus geometry to responses, we first determined the spatial position of each cell's direct input from photoreceptors by examining L2 responses to a bright bar moving across a dark background. As expected, L2 cells first hyperpolarized when the bar reached the RF center, causing a local light increment (Figure 1B) and then depolarized as the bar moved away, causing a local light decrement. The spatial coordinates of the RF center were identified by relating the timing of each response to the bar's position (Figure S1A available online). This procedure was performed for all cells and only cells that had RF centers on the screen were considered for analysis.

We next presented L2 cells with flashes of light covering the entire screen. Interestingly, individual cell responses to this seemingly simple stimulus varied in polarity, shape, and kinetics (Figure S1B). These responses changed progressively across individual terminals, following retinotopic shifts in RF position (Figures S1C–S1E). These observations demonstrated that L2 cells with RF centers directly under the stimulus hyperpolarized to light, while cells at the periphery of the screen, whose centers were not directly stimulated by light, depolarized. We inferred that cells that depolarized to light responded to lateral antagonistic inputs rather than to direct inputs from photoreceptors. To directly relate responses to the spatial pattern of light, we generated a "partial field flash" stimulus in which only a portion of the screen was transiently brightened or darkened. To compare responses across conditions, we defined a response strength metric as the mean response amplitude to light increments and decrements and set the sign of this metric, by convention, to be negative for cells that hyperpolarized to light (Figures S1F and S1G, Supplemental Experimental Procedures). This analysis showed that cells with RF centers inside the flash region hyperpolarized to brightening and depolarized to darkening, while cells with RF centers outside this region responded with opposite polarity (Figures 1C and 1D). Thus, individual cells produced responses of opposite polarities to center and surround stimulation, as well as to decrements and increments.

Behavioral responses to motion of rotating square-wave gratings display a contrast frequency optimum between 5–10 Hz (Tammero et al., 2004; Clark et al., 2011). To assess whether surround responses were sufficiently fast to shape signals relevant to motion vision, we presented brief "partial field flashes" (Figures 1E and 1F). For flashes lasting 200 ms, cells responded with opposite polarity to center and surround stimulation. Both response types were biphasic and largely differed in amplitude rather than kinetics (Figure 1F). The response shape was consistent with kernels extracted from L2 responses to dynamically varying noise stimuli (Clark et al., 2011). Thus, surround inputs influence L2 responses even to rapid stimuli, on timescales that impact motion detection.

The L2 RF Has a Narrow Center and an Extended Surround

We next examined how L2 responses vary as a function of the extent of center and surround stimulation by presenting circles and annuli, of either contrast polarity, around identified RF centers (Figures 2 and S2). As expected from an antagonistic center-surround RF, responses to large circles were weaker than those to small circles (Figures 2A–2D, S2A, and S2B). In addition, annuli with sufficiently large internal radii so as to reduce center stimulation (4° and above) produced inverse responses (Figures 2E, 2F, and S2C–S2F). We infer that surround effects become stronger than center effects approximately 5° away from the RF center and extend radially to more than 15°. We next quantified the effects of surround stimulation by computing response amplitudes as a function of the spatial extent of the stimulus (Figures 2C, 2D, S2E, and S2F; as described in S1F). This analysis showed that the relative effect of surround stimulation differed between increments and decrements. For increments, amplitudes of responses to large circles were ~50% smaller than responses to small circles ($p < 10^{-4}$), while for decrements they were not statistically significantly different (Figures 2C and 2D). We next tested whether L2 responses reflect linear spatial integration. To do this, we compared responses evoked by combined center and surround stimulation with linear summation of responses to each individual component. For many such combinations, linearly predicted responses significantly differed from measured responses, particularly for contrast decrements (Figures 2G and 2H). Thus, the L2 RF is nonlinear in space.

Lateral Antagonism Links Spatial Structure to Response Kinetics

Responses to circles and annuli revealed that surround inputs affect not only response strength but also its kinetics. We quantified these effects by comparing mean response values at different time points during stimulus presentation (Figures 3 and S3). For small circles, response amplitudes changed very little during stimulus presentation, while for large circles, significant decreases in amplitude were observed (Figures 3A–3D). As more inhibition was provided together with excitation, responses became more transient (Figures 3A, 3B, and S3A–S3D). As a result, the spatial RF shape effectively became sharper over time, particularly in responses to dark circles (Figures 3C, 3D, S3C, and S3D). In contrast, all hyperpolarizing responses decayed. Thus, it is possible that a mechanism that makes hyperpolarizing responses to increments transient, such as extracellular potentials within the lamina cartridge (Weckström and Laughlin, 2010), does not act similarly on depolarizing responses to decrements. Accordingly, only depolarizations require surround inputs for transience. However, an imbalance in the relative strengths of increment versus decrement stimuli may also play a role in determining decay rates.

A separable spatiotemporal RF is described by the multiplication of a temporal filter with a spatial filter (Shapley and Lennie, 1985). With such an RF, responses to circles of different sizes are predicted to vary in scale but not in kinetics. However, as we observed that decay rates increased with surround stimulation, the L2 RF must be spatiotemporally coupled. Interestingly, spatiotemporal coupling can also be observed in responses to annuli, particularly dark ones (Figures 3E–3H). Plotting the mean response values at different time points during the presentation of annuli of different sizes revealed that, at the edge of the RF center, responses grew stronger over time instead of decaying (left box, Figure 3G). Thus, responses to dark annuli with internal radii of 4° or 6° were initially hyperpolarizing (blue curves in Figure 3G), and the extent of hyperpolarization increased during the response (red curves in Figure 3G). That is, surround responses next to dark edges were sustained, effectively enhancing their contrast. Interestingly, surround responses further away from dark edges, near similarly responding cells, were more transient (right box, Figure 3G). This suggests that L2 responses are shaped by inputs from neighboring columns regardless of whether these columns are directly stimulated by light or are responding to more lateral inputs. These results argue that models of L2 responses should include two components: one component that gives rise to a sustained center or surround response and another component that transforms the sustained response to a transient one.

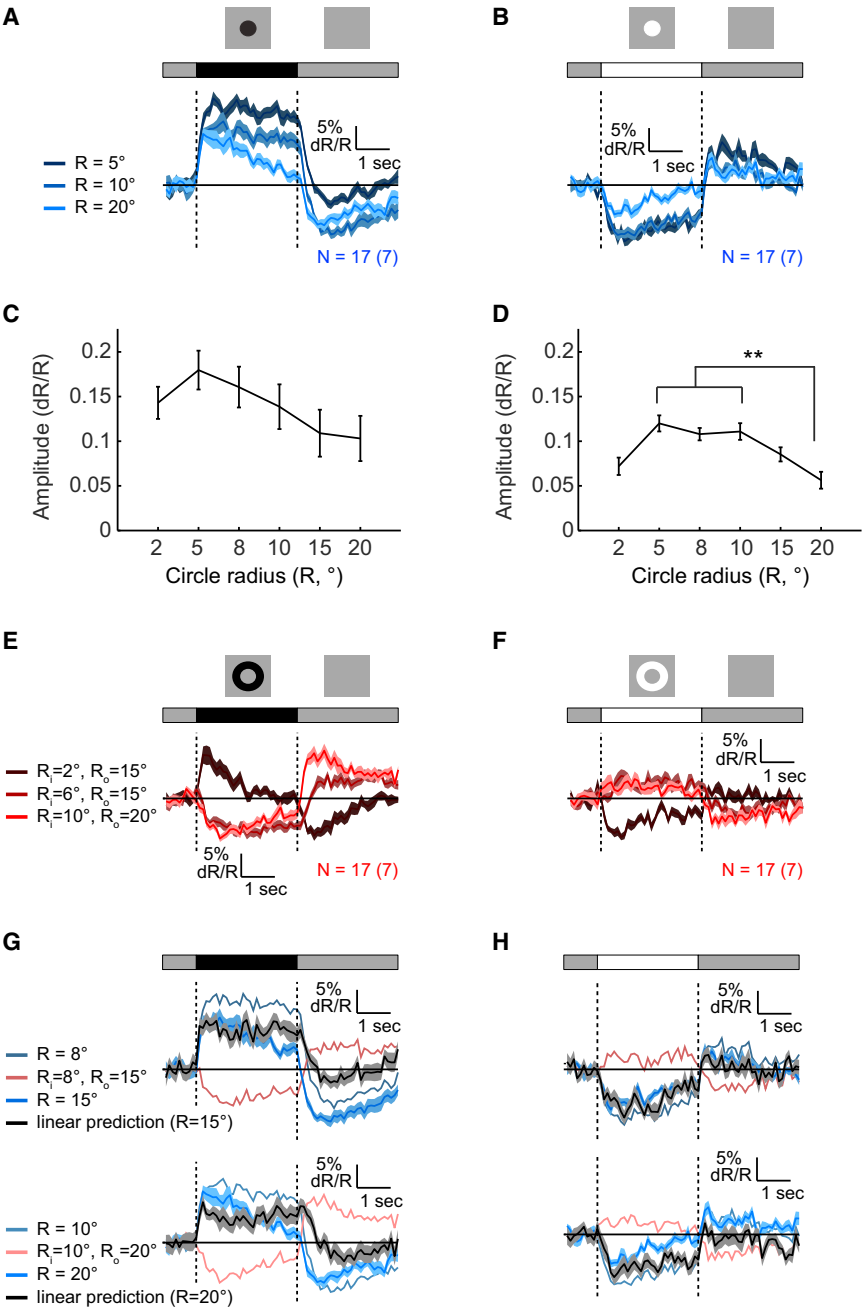

Figure 2. Responses to Circles and Annuli Reveal the Spatial Shape of the RF

(A–F) Mean responses to dark (A and E) and bright (B and F) circles (blue traces, A and B) and annuli (red traces, E and F) of different sizes presented for 3 s on an intermediate illumination level background, around identified RF centers. Shading here and in (G) and (H) denotes ±1 SEM.

(C and D) Mean amplitudes of responses to dark (C) and bright (D) circles, as a function of the radius, R. ** indicates a significant difference between the two means by one-way ANOVA, according to Tukey's honestly significant difference criterion (D). Error bars denote ±1 SEM.

(G and H) Comparing predicted responses (black continuous traces) to measured responses (blue continuous traces) to the presentation of a 15° circle (top) and a 20° circle (bottom), assuming linearity, as a sum of responses to circles and annuli of appropriate sizes. Dark stimuli responses (G) and bright stimuli responses (H) are shown. See also Figure S2.

A Simple Model Captures L2's Inseparable Spatiotemporal RF

To assess whether the variability in decay rates observed in responses to dark stimuli could arise via simple mechanisms, we constructed a quantitative model. Previous work demonstrated that a weighted sum of two opposite-signed inputs with different time constants can produce responses with different decay rates (Rodieck, 1965; Richter and Ullman, 1982; Fleet et al., 1985; Fleet and Jepson, 1985). Thus, we constructed a model comprising two inputs: a primary input associated with a fast rising exponential and an antagonistic input associated with a slowly decaying exponential (Figure 4A). With appropriate weights, a fast rising and gradually decaying response, similar to the response to the presentation of a large dark circle, was produced. We next tested whether the model's weights and time constants could be appropriately tuned to different L2 responses. Indeed, increasing the weight of the antagonistic component decreased the response amplitude and increased its decay rate (Figure S4A), as observed in L2 responses to circles of increasing sizes (Figures 2A and S2A). Interestingly, delaying the development of the antagonistic input by increasing the time constant of the exponential decay produced both increased amplitudes as well as reduced decay rates because the excitatory response could develop further before inhibition suppressed it (Figure S4B). To fit L2 responses with this model using a small parameter set, we assumed that each input is associated with a circularly symmetric Gaussian structure over space (Figure 4B). The weight of each model component was set by appropriately integrating over this structure. As a result, predictions of both responses to circles and annuli were based on a difference of Gaussians spatial model structure (Figures 4C and S4C). We first fitted this model to responses of L2 cells to dark circles of variable sizes (Figure 4D and Supplemental Experimental Procedures). The primary input in these responses was associated with the RF center and the antagonistic input with the surround. Next, responses to dark annuli with large internal radii (>4°) were fitted with the same model using different parameters (Figure 4E). The primary model component in this case corresponded to a surround while the

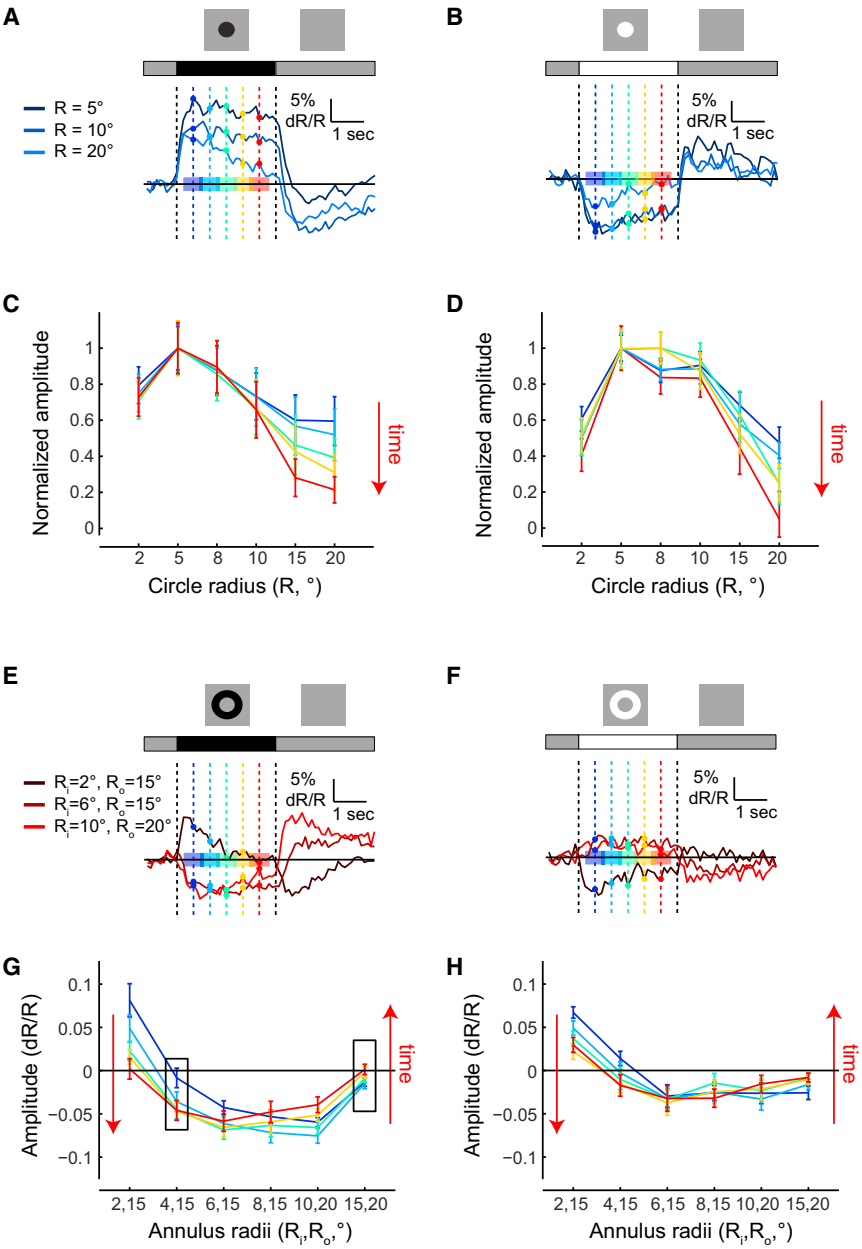

Figure 3. Surround Stimulation Modulates Response Kinetics

(A and B) Mean responses to dark (A) and bright (B) circles of different sizes as a function of time. Dark blue, mean responses to small circles; bright blue, mean responses to large circles. Amplitudes were measured for the different responses at different time points, shown as vertical lines and sample points in different colors. Average amplitudes were computed over the intervals indicated by colored patches. Cold colors, early stages of the response; warm colors, late stages.

(C and D) Normalized amplitudes of responses to dark (A) and bright (B) circles of different sizes as a function of their radius R, at different time points during the response. Each curve is normalized to the maximal response strength over all radii. Error bars denote ±1 SEM.

(E and F) Same as (A) and (B), describing responses to dark (E) and bright (F) annuli of different sizes.

(G and H) Same as (C) and (D), describing the strength of responses to dark (G) and bright (H) annuli of different sizes, without normalization. See also Figure S3.

antagonistic component was a surround antagonist that caused surround responses to decay. The different parameters accounted for the spatial nonlinearity of the L2 RF (Figures 2G and 2H), as well as the different kinetics of decaying center and surround responses (Figures 1D, 2A, 2B, 2E, 2F, S2A–S2D, and S4D). Thus, the primary surround input giving rise to responses to annuli was stronger, and had a shorter time constant, than the antagonistic input that suppressed responses to center stimulation (Tables S1 and S2). However, in spite of amplitude and kinetics differences, both these inputs were fit by the same spatial parameter, which is probably set by the columnar structure of the eye. Finally, the surround antagonist component had a broad spatial extent and a time constant similar to that of the antagonistic input in the circle response model. We hypothesize that this component is mediated by lateral inputs from columns in which surround responses occur. Overall, the fits to the six circles and four annuli responses explained 98% of the variance (Figures 4D and 4E). However, fitting responses to annuli with small internal radii (2° and 4°) that provide partial center stimulation and significant surround stimulation required a distinct weighting of inputs (Figure S4E and Supplemental Experimental Procedures). In contrast, most responses to bright circles of different sizes could be captured simply as scaled versions of the same response shape (Figure S4F).

Lateral Antagonism Creates Anisotropic Acuity

A center-surround RF differentially affects the amplitudes of responses to stimuli with different spatial periods (e.g., Dubs, 1982). Thus, the relative strengths of responses to sinusoidal inputs with different periods provide a measure of acuity. Acuity differences between different axes may represent an early specialization for the detection of motion in a particular orientation (Srinivasan and Dvorak, 1980). We therefore measured L2 responses to sinusoidal gratings with periods ranging from 5° to 90°, presented on a virtual cylinder. Each grating was rotated at a different speed so that the temporal contrast frequency was 0.5 Hz and was oriented to simulate either pitch or yaw rotations of the fly (Figure 5A). L2 responses to these stimuli were sinusoidal, as expected for a linear system (Figure 5B; Clark et al., 2011). Intriguingly, at short spatial periods

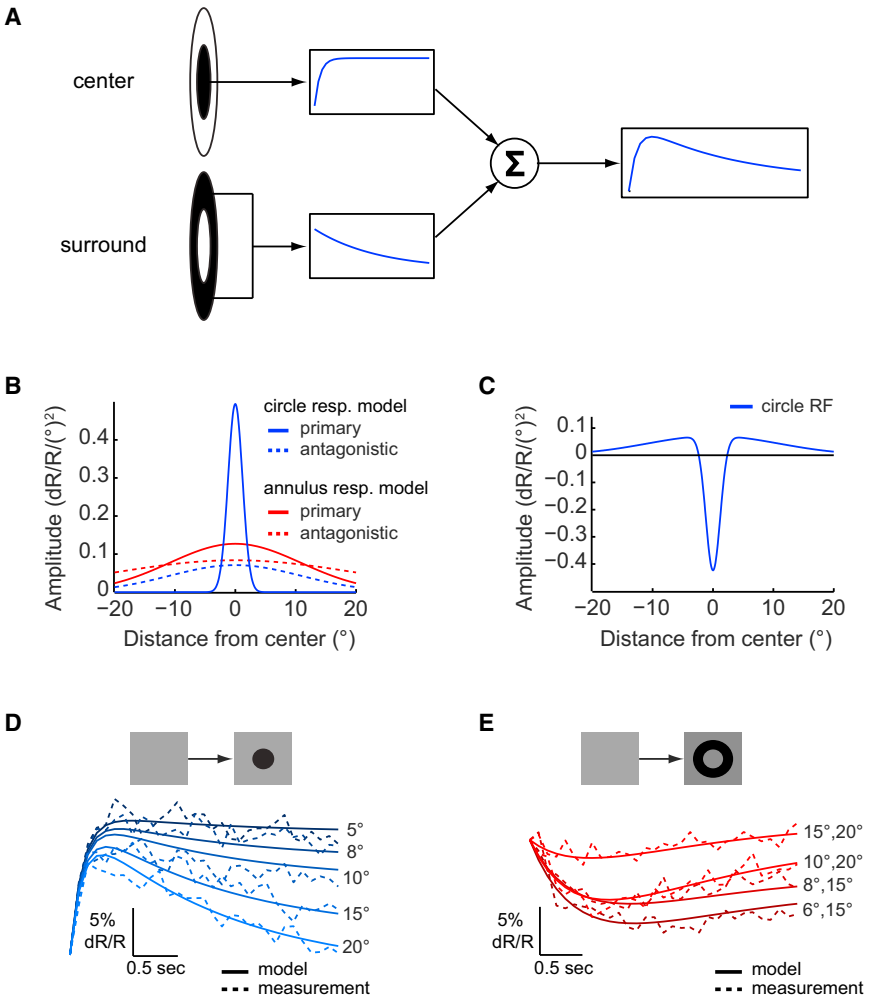

Figure 4. Spatiotemporal Inseparability Can Arise from a Combination of Inputs Associated with Different Timescales

(A) A schematic description of the model. The primary component, arising from stimulation of the RF center, is associated with a fast rising exponential (top); the antagonistic component, arising from stimulation of the RF surround, is associated with a slow decaying exponential (bottom). These two inputs are summed to give rise to the response.

(B) The strength of the primary (continuous traces) and antagonistic (dashed traces) components over space used to set the weights of these components in simulations of circle (blue) and annuli (red) responses.

(C) The RF shape inferred from the spatial distribution of component strengths used in modeling responses to circles.

(D) Simulated (continuous) and measured (dashed) responses to dark circles of variable sizes. Dark blue, small circles; light blue, large circles (as in Figures 2 and S2).

(E) Simulated (continuous) and measured (dashed) responses to annuli of variable sizes; dark red, annuli with small internal radii; bright red, annuli with large internal radii (as in Figures 2 and S2). See also Figure S4.

(10° and 20°), responses to pitch rotations were stronger than responses to yaw rotations ($p < 10^{-5}$, Figures 5B and 5C). At a 5° spatial period, responses were weak, as expected from retinal optics and an RF center of approximately 5° (Järvilehto and Zettler, 1973; Stavenga, 2003), while spatial periods around 40° drove the strongest responses (Figure 5C). Only slight attenuation by surround inhibition was observed at larger spatial periods (Figure S5A). This could be for physiological reasons, arising, for example, from effects of the relative timing of center and surround stimulation on antagonism. However, this could also result from technical limitations, as our display spanned slightly less than 60° of visual space in each direction. Nevertheless, as responses at short spatial periods clearly show higher sensitivity with pitch rotations, visual acuity must be higher around this axis, making the L2 RF spatially anisotropic. Analogous results were obtained using a moving bright bar stimulus, which weakly stimulated the surround prior to entering the RF center, and induced a stronger surround response when it moved upward across the screen than when it moved medially (Figures 1B, S1A, S5B, and S5C).

GABAergic Inputs to R1–R6 Photoreceptors Provide Surround Signals in L2

To explore circuit mechanisms shaping L2 responses, we developed a procedure for rapidly characterizing the spatial RF using sequential presentations of a dark, stationary, 10° wide bar, oriented horizontally or vertically at different positions. To extract an RF shape description with high spatial resolution, we took advantage of the random distribution of distances of different cell RFs from the bar's nearest edge. Responses were aggregated by this distance, combining responses of cells that experienced equivalent RF stimulation (Figure 6A). We also aggregated responses to bars with different orientations, as the effect of the anisotropic RF shape on these maps was small (but significant; $p = 0.0014$, χ^2 test; Figure S6A). As expected, cells having RF centers within the bar transiently depolarized when the bar was presented, while cells having RF centers outside the bar responded with inverse polarity (Figures 6B and 6C). To extract a proxy of the spatial RF shape, we plotted response strength, measured as the mean response amplitude evoked by the onset and offset of the bar (as in Figure S1F), as a function of the distance from the edge (Figure 6D).

We next examined whether GABA mediated surround responses. We took advantage of RNA interference (RNAi) constructs directed against both $GABA_A$ and $GABA_B$ receptors ($GABA_A$Rs and $GABA_B$Rs, respectively), expressed cell-type specifically using the Gal4-UAS system (Liu et al., 2007; Root et al., 2008). Knockdown of both GABARs in L2 cells had no effect on the spatial RF shape (Figure S6B). However,

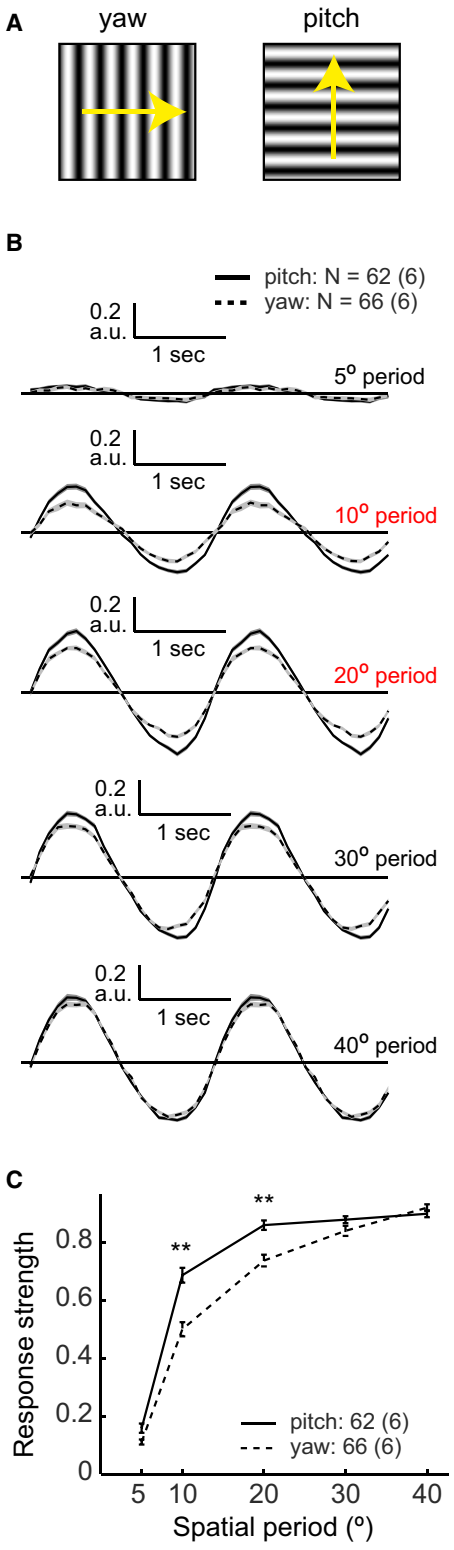

Figure 5. Lateral Inhibition Gives Rise to an Acuity Difference between Orientations

(A) Schematic description of the stimulus: sinusoidal contrast gratings moving around the yaw (left) and pitch (right) axes.

knockdown of GABARs simultaneously in both R1–R6 photoreceptors and L2 cells increased the effective size of the RF center and decreased the strength of surround responses (Figures 6E, S6C, and S6D). Thus, GABAergic input onto L2's presynaptic partner, the photoreceptors, shapes the L2 RF surround. Interestingly, neither knockdown of $GABA_A$Rs or $GABA_B$Rs alone changed the RF shape (Figure S6E). Thus, both receptors are redundantly required to mediate surround responses.

Since these manipulations did not completely eliminate surround responses, we examined whether GABARs on more distant cells might have additional effects. We therefore applied the $GABA_A$R and $GABA_B$R antagonists, picrotoxin (125 μM) and CGP54626 (50 μM), simultaneously (Olsen and Wilson, 2008; Root et al., 2008). Under these conditions, the normalized strength of surround responses with respect to center responses significantly decreased (Figure 6F). This effect was similar, yet stronger, from that observed by knocking down these receptors using RNAi in photoreceptors and L2. To define the distinct contribution of the ionotropic $GABA_A$Rs and the metabotropic $GABA_B$Rs to L2 responses, we applied picrotoxin and CGP54626 separately. Interestingly, application of the $GABA_A$R antagonist alone was sufficient to suppress the RF surround as strongly as the two antagonists combined (Figure 6F), while application of the $GABA_B$R antagonist alone had no effect on the spatial RF shape (Figure S6F). Taken together, these genetic and pharmacological manipulations demonstrate that GABAergic circuits play a critical role in establishing the spatial RF shape of L2. As the pharmacological block of $GABA_A$Rs strongly suppressed surround responses, while the knockdown of $GABA_A$Rs alone had no effect, we infer that these manipulations act on overlapping but distinct circuit targets. We note that surround responses were not completely eliminated, even by the broad pharmacological manipulations. We infer that either these antagonists had only partial access to the brain or additional, nonsynaptic mechanisms may also contribute. Thus, multiple circuit components are probably involved in constructing L2's extensive surround.

GABAergic Inputs Are Required for L2 to Respond to Contrast Decrements

GABAergic manipulations affected not only the spatial RF shape of L2 but also the amplitudes and kinetics of responses (Figures 6G, 6H, and S6G–S6J). We thus examined these effects in greater detail. During responses to moving bright bars on dark backgrounds, L2 transiently hyperpolarized as the bar reached the RF center, causing a local light increment, and depolarized as it moved away, causing a local light decrement (Figures 1B and 7A–7C, top). Similarly, during responses to static dark bars, L2 cells with RF centers in the bar transiently depolarized

(B) Normalized mean responses to moving sinusoidal gratings with different spatial periods, moving around the pitch (continuous) and yaw (dashed) axes. Responses were normalized to the maximal response amplitude across all spatial periods. Shading denotes ±1 SEM.

(C) Response strength as a function of the spatial period of the grating moving around the pitch (continuous) and yaw (dashed) axes. Error bars denote ±1 SEM. **$p < 0.001$ in a two-tailed Student's t test with unequal variances. See also Figure S5.

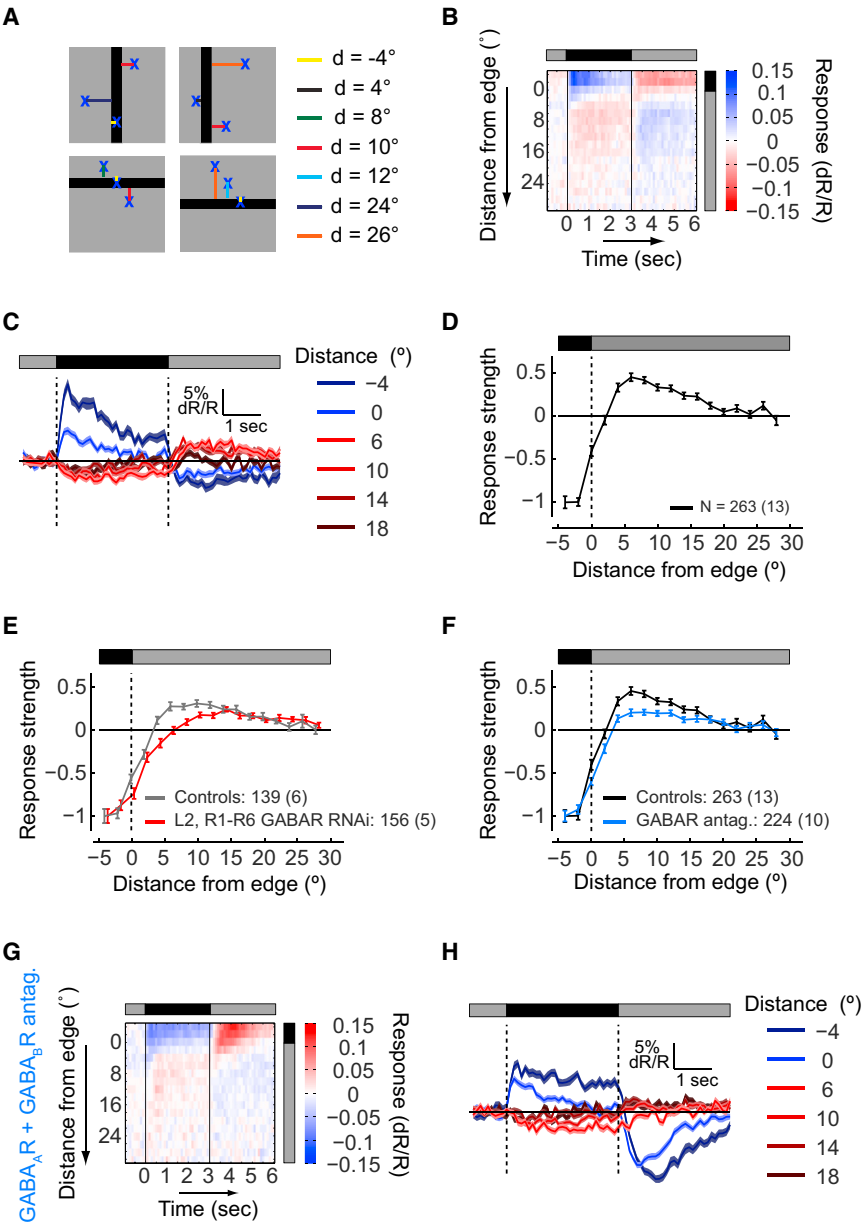

Figure 6. GABA Receptors in Photoreceptors Contribute to the Inhibitory Surround

(A) Schematic illustration: a dark bar is presented at a random position on a background of intermediate illumination, while responses are aggregated by the distance of RF centers from the bar's edge. Negative distances correspond to RF centers within the bar.

(B) The mean response of L2 cells as a function of the distance of the RF center from the bar's edge and the bar presentation time. Response (dR/R) values encoded as described by the color scale.

(C) The mean response to the presentation of the bar at different distances between the RF centers and the bar's edge, as a function of time. Blue, mean responses of cells with RF centers within the bar presentation region; red, mean responses of cells with RF centers outside the bar presentation region. Shading denotes ±1 SEM.

(D) Mean response strength as a function of the distance from the bar's edge, normalized to the strength at a distance of 4°, within the bar. Negative strength values correspond to depolarization during the bar presentation, positive values to hyperpolarization. Here and in (E) and (F), error bars denote ±1 SEM.

(E and F) The effects of manipulations on the mean response strength as a function of the distance from the bar's edge.

(E) Gray, controls; TN-XXL expressed in L2 and in R1–R6 photoreceptors; red, experiment, knockdown of GABA$_A$Rs and GABA$_B$Rs in L2 and R1–R6 photoreceptors.

(F) Same as (E); black, controls; TN-XXL expressed in L2 cells only; blue, experiment, application of GABA$_A$R and GABA$_B$R antagonists.

(G and H) Same as (B) and (C), after application of GABA$_A$R and GABA$_B$R antagonists. See also Figure S6.

when the bar was presented and hyperpolarized to a sustained level when it was eliminated (Figures 6C and 7A–7C, bottom). Application of GABAR antagonists enhanced the hyperpolarizing responses to increments and suppressed the depolarizing responses to decrements in both stimuli (Figure 7A). In addition, in the presence of antagonists, the depolarizing response to the static bar presentation decayed slowly, as anticipated by our previous observations that decay rates of decrement responses depend on stimulation of the RF surround mediated via GABA receptors (Figures 2, 3, and 6). In contrast, the hyperpolarizing response was no longer sustained. Interestingly, the decrease in the amplitude of the response to the light decrement and increase in the response to the increment cannot be explained by reduced surround effects. Thus, GABAergic circuits must play an additional role in shaping L2 cell responses to light inputs, specifically mediating responses to light decrements while inhibiting increment responses. Application of either the GABA$_A$R or the GABA$_B$R antagonist alone suppressed depolarizing responses to decrements (Figures 7B and 7C), contributing to the combined effect, but neither enhanced hyperpolarizing responses. In addition, both GABA$_A$R and GABA$_B$R antagonists made the hyperpolarizing response to the elimination of the static bar more transient, but only the GABA$_A$R antagonist made the depolarizing response to the bar presentation more sustained, consistent with surround suppression by this receptor only.

Knockdown of both GABARs in L2 cells and R1–R6 photoreceptors did not have a significant effect on the shapes of responses to either static or moving bar stimuli (Figure 7D). Knockdown of GABA$_A$Rs in these cells enhanced the depolarizing response to light decrements (Figure 7E). In contrast, knockdown of GABA$_B$Rs suppressed the depolarizing response to decrements and made the hyperpolarizing response less

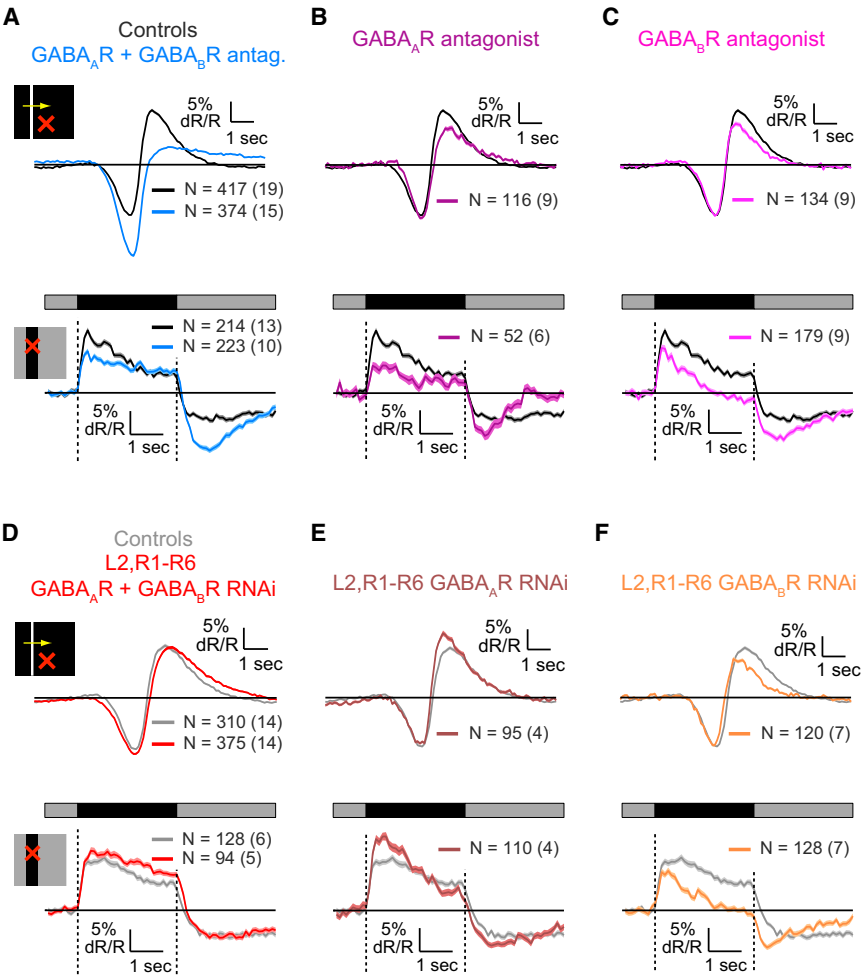

Figure 7. GABAergic Circuits Mediate OFF Responses in L2 Cells

(A–F) Mean response of controls and experimental cells to a moving bright bar on a dark background (top) and to a dark bar on an intermediate illumination level background (bottom), for cells with RF centers within the bar. In all figure panels, shading denotes ±1 SEM.

(A–C) Black, controls, TN-XXL expressed in L2 cells only.

(A) Blue, application of GABAR antagonists.

(B) Purple, application of the GABA$_A$R antagonist picrotoxin.

(C) Magenta, application of the GABA$_B$R antagonist CGP54626.

(D–F) Knockdown of receptors in L2 cells and R1–R6 photoreceptors. Gray, controls, TN-XXL expressed in L2 cells and R1–R6 photoreceptors.

(D) Red, knockdown of GABARs.

(E) Brown, knockdown of GABA$_A$Rs.

(F) Orange, knockdown of GABA$_B$Rs.

sustained (Figure 7F). These effects were indistinguishable from those caused by pharmacological block of the same receptors (Figure 7C). Thus, the effect of GABA$_B$Rs on the shape of L2 cell responses to light decrements and increments is mediated via receptors on either L2 or photoreceptors, or both. The difference between the combined effect of GABA$_A$R and GABA$_B$R antagonists and the genetic knockdown of both receptors may be explained by the cancellation of opposing effects of individual receptor knockdowns on decrement responses. This is also consistent with the notion that the effect of pharmacological block of GABA$_A$Rs is due to receptors distinct from those in L2 cells and photoreceptors. Overall, these results demonstrate that GABAergic circuits play a significant role in regulating the amplitude and kinetics of L2 responses to both light increments and decrements applied to the RF center, in addition to mediating surround responses.

GABAergic Circuits Linearize Responses to Contrast Changes

These results implied that GABAergic inputs might enable L2 to balance responses to light increments and decrements. To test this hypothesis, we examined whether the linearity of L2 responses to sinusoidal contrast changes was affected by the application of GABAR antagonists. Indeed, this manipulation significantly altered the responses, as the responses to the brightening and darkening phases of this stimulus were no longer similar in amplitude (Figures 8A–8C). In particular, the hyperpolarizing response to light increments became significantly larger, while the depolarizing response to decrements failed to track the darkening input and displayed saturation (Figure 8A). We quantified this deviation from linearity by computing the differences between measured responses and sinusoids with matched amplitudes. Larger deviations were found following addition of GABAR antagonists (Figures 8B and 8C). The same effect on linearity was observed in response to stimuli moving around either the pitch or yaw axes (Figures S7A–S7C). However, knockdown of GABARs in L2 and photoreceptors increased the linearity of responses to sinusoidal gratings (Figures S7D–S7F). Nevertheless, both application of GABAR antagonists and knockdown of GABARs in L2 cells and photoreceptors suppressed the differences between the amplitudes of responses to gratings moving around the pitch and yaw axes (Figures S7G and S7H). Thus, as the knockdown of GABARs mediates surround effects but does not affect contrast polarity sensitivity, these observations suggest that, under these stimulus conditions, surround effects decrease the linearity of L2 responses to contrast. When GABARs are broadly blocked by antagonists, the small, positive effect of blocking GABARs in L2 and photoreceptors on linearity is overwhelmed by the much larger negative effect induced by the change in contrast polarity sensitivity mediated by a different circuit component. Thus, the role of GABAergic circuits in regulating contrast polarity sensitivity, not surround responses, is critical for linearizing responses to contrast in L2.

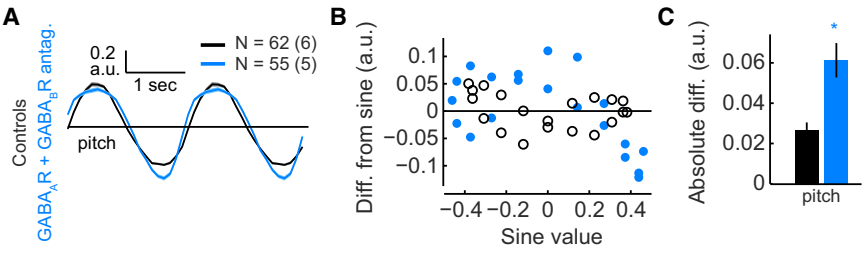

Figure 8. GABAergic Circuits Linearize L2 Responses to Contrast

(A) Mean responses to sinusoidal gratings with a spatial period of 40° moving around the pitch axis. Shading denotes ±1 SEM.

(B) The difference between the measured mean response and a reference sinusoidal response with the same maximal amplitude, as a function of the reference response value.

(C) The mean absolute difference across all response values presented in (B). *$p < 0.05$ in a two-tailed Student's t test with unequal variances. Error bars denote ±1 SEM. See also Figure S7.

DISCUSSION

Our results reveal a nonlinear, spatiotemporally coupled center-surround antagonistic RF structure in L2 cells that mediates different responses to dark or bright inputs of different sizes. These functional properties must affect the computations performed by downstream motion processing pathways and make the outputs of elementary motion detectors (EMDs) depend on the geometry and contrast of moving objects. Using pharmacological and genetic manipulations, we reveal that GABAergic circuitry, including presynaptic inhibition via GABARs on photoreceptors, mediates lateral antagonistic effects on L2. Moreover, these circuits are required for L2 to respond strongly to decrements, enabling the downstream circuits to become specialized to detect moving dark edges. Remarkably, our detailed characterization of L2 reveals that many visual processing properties are shared with first-order interneurons in the vertebrate retina. These strikingly similar computational properties arise via distinct molecular mechanisms, arguing strongly for evolutionary convergence.

L2 Cells Have an Antagonistic, Anisotropic Center-Surround Receptive Field

The L2 RF displays an antagonistic center-surround organization over space (Figures 1 and 2), consistent with electrophysiological studies in larger Diptera (Dubs, 1982; Laughlin and Osorio, 1989). The RF center has a radius of 3°–5°, while the surround peaks approximately 10° away from the center and persists as far as 15° or more away. Importantly, this spatial RF is nonlinear. Center responses dominate surround antagonism such that responses to surround stimulation alone are stronger than predicted from suppression of center responses by surround inputs. Furthermore, the kinetics of surround responses differ from the effect of surround inputs on center responses.

Our data demonstrate that surround antagonism affects the spatial frequency tuning of L2 outputs, reflecting higher acuity for stimuli rotating around the pitch axis compared to the yaw axis (Figures 5 and S7). Thus, fine spatial features are better captured when they are separated around this axis. Similar anisotropic center-surround RF structures were identified in LMCs of flies and other arthropods (Barlow, 1969; Arnett, 1972; Johnston and Wachtel, 1976; Mimura, 1976; Srinivasan and Dvorak, 1980; Dubs, 1982; Glantz and Bartels, 1994). We note, however, that our measurements focused on a particular dorsal and medial region of the eye. Thus, it remains possible that a distribution of spatial orientation sensitivities exists across the eye, analogous to the optic-flow sensitivity fields of motion-sensitive neurons (Weber et al., 2010).

The L2 RF Is Spatiotemporally Coupled yet Can Be Captured by a Simple Model

Lateral antagonistic signals in L2 responses enhance spatial and temporal contrast by generating a biphasic filter in both space and time, consistent with efficient contrast encoding theories (Ratliff et al., 1963; Laughlin, 1994; Srinivasan et al., 1982; van Hateren, 1992). However, while such theories often presume linearity and spatiotemporal separability, L2 responses are inconsistent with these assumptions. In particular, response kinetics depend on the spatial properties of the stimulus and its contrast polarity (Figure 3; Laughlin, 1974b; Mimura, 1976; Laughlin and Osorio, 1989; van Hateren, 1992). This spatiotemporal inseparability can be captured by a computational model that combines two linear and separable inputs (Richter and Ullman, 1982; Fleet et al., 1985). The fitted model consists of two different sustained components, with distinct time constants, representing primary and antagonistic inputs (Figure 4). With this model, the spatial nonlinearity of L2 is captured by utilizing different amplitudes and time constants of antagonism, depending on whether the RF center is stimulated. For all responses, the decay rate is determined by the strength of the antagonistic component. Thus, L2 responses are affected by interactions with neighboring columns, regardless of whether those columns receive input from stimulated photoreceptors or from lateral pathways.

The Spatiotemporally Coupled L2 RF Efficiently Encodes Dark Object Motion Cues

L2 represents a critical input to a neural circuit that detects moving dark edges (Joesch et al., 2010; Clark et al., 2011). Interestingly, the characteristics of L2 responses to decrements are useful for encoding motion-related cues (Figure 9A). Motion transforms the spatial structure of an object moving in front of a photoreceptor array into a temporal pattern of activity in each detector. Thus, small objects give rise to brief cues, observed only by a few detectors at any given time. Such small, local signals are difficult to distinguish from noise. In contrast, large objects give rise to sustained cues, simultaneously observed by many detectors. Such cues include significant redundancies in space and time that inhibition is expected to reduce (Barlow, 1961; but see Pitkow and Meister, 2012). The responses of L2 are useful for capturing the motion of both types of

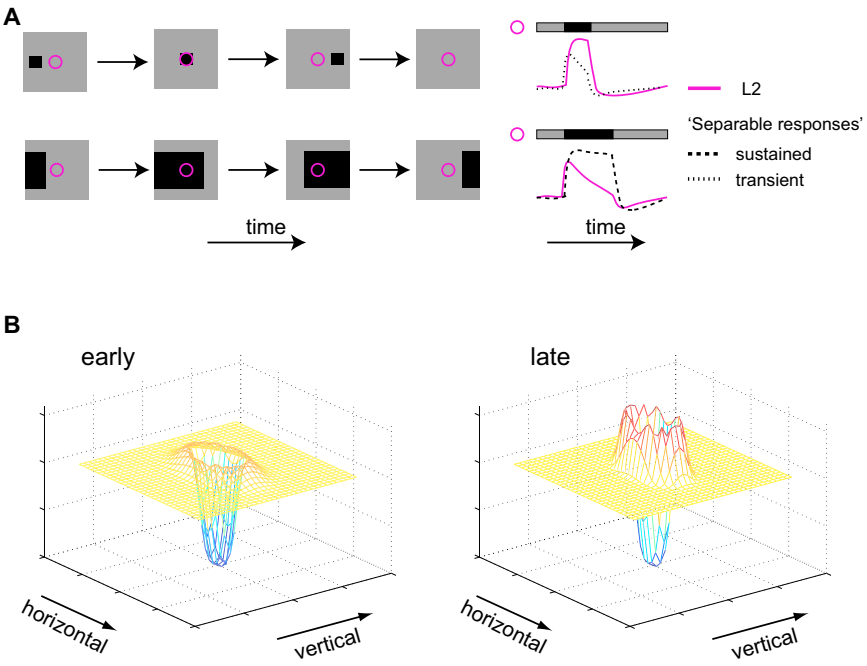

Figure 9. L2 RFs Are Anisotropic, Spatiotemporally Coupled, and Efficiently Capture Cues Associated with Dark Object Motion

(A) Schematic representation of the utility of L2 RF's spatiotemporal coupling to motion encoding. Left column: example stimuli as a function of time. Purple circle: the RF center of an L2 cell. Right column: schematic responses to stimuli as a function of time. Purple, illustrative L2 responses, spatiotemporally coupled. Black, illustrative responses of hypothetical cells with spatiotemporally separable RFs. Dotted (top), illustrative response of a hypothetical cell with transient responses. Dashed (bottom), illustrative response of a hypothetical cell with sustained responses.

(B) Schematic representation of the two-dimensional L2 RF at an early (left) and late (right) stage of the response to a stimulus, capturing its anisotropy in space with gradually increasing surround lobes.

objects. In particular, responses to small dark objects are sustained, enhancing evoked signals, while responses to large dark objects rapidly decay, encoding the contrast changes associated with edge motion and reducing redundancy (Figures 2A, S2A, and 9A). Separable RFs cannot implement this response duality because such filters give rise to identical response kinetics for all objects (Figure 9A). Finally, as a result of delayed surround effects, the spatial shape of L2 RFs varies over time, with inhibition becoming gradually stronger (Figure 9B).

The L2 RF Has Implications for Elementary Motion Detection

A central model of elementary motion detection correlates two local inputs that each relay contrast information from a single point in space with a relative time delay (Hassenstein and Reichardt, 1956). Filtering of these inputs prior to multiplication critically affects EMD outputs (Borst et al., 2003; Eichner et al., 2011). L1 and L2 provide inputs to EMDs and thus their outputs must represent some of these filtering stages (Rister et al., 2007; Joesch et al., 2010; Clark et al., 2011). We show that L2 outputs are strongly shaped by the light distribution across a broad region in space and by contrast polarity. Thus, the kinetics and amplitudes of L2 outputs differ for bright and dark objects of different shapes and sizes. Consequently, probing EMDs with minimal motion cues that differ in contrast and spatial extent could produce different results due to differential input filtering rather than differences in motion detection per se (Hassenstein and Reichardt, 1956; Egelhaaf and Borst, 1992; Eichner et al., 2011; Clark et al., 2011). More generally, spatiotemporal coupling observed in L2 can give rise to speed tuning, differentially regulated for bright and dark objects, and thus affect tuning of downstream EMDs to different speeds or to dark or bright motion cues (Fleet et al., 1985; Fleet and Jepson, 1985; Egelhaaf and Borst, 1989; Srinivasan et al., 1990; Juusola and French, 1997; Zanker et al., 1999). Finally, the surround responses of L2 effectively convert a contrast increment at one spatial location into depolarizing responses at neighboring locations, providing a route by which increment information could enter a dark edge-detecting pathway, even given downstream half-wave rectification (Clark et al., 2011).

Lateral GABAergic Circuits Give Rise to the Center-Surround Organization of the L2 RF

Anatomical studies describe a dense network of connections in the lamina (Meinertzhagen and O'Neil, 1991; Rivera-Alba et al., 2011). Here we show how GABAergic circuits within this network shape the functional properties of L2 (Figures 6, 7, and 8). Photoreceptors receive direct GABAergic input that depends on both $GABA_A$Rs and $GABA_B$Rs and shapes the RF surround in L2 (and presumably other LMCs). $GABA_A$R-dependent synapses elsewhere in the circuit relay surround inputs into photoreceptors. A possible surround input is the centrifugal cell, C3, the only cell that is both presynaptic to photoreceptors and GABAergic (Buchner et al., 1988; Kolodziejczyk et al., 2008; Rivera-Alba et al., 2011). Furthermore, since our genetic manipulation of GABARs affected both L2 cells as well as photoreceptors, we cannot exclude the possibility that receptors on both cells are redundantly required. Thus, the GABAergic centrifugal cell C2, which is presynaptic to L2, could provide these inputs. Additional $GABA_A$Rs have been identified in L4 and another wide-field tangential cell (Enell et al., 2007; Kolodziejczyk et al., 2008) and could mediate the distal effects of manipulating $GABA_A$Rs.

Modulation of GABAergic signaling in L2 expands the RF center and increases spatial pooling. Such a change in RF shape increases signal-to-noise ratios and occurs under low light level conditions (Dubs et al., 1981; Dubs, 1982). Thus, we speculate that one role of GABAergic inputs may be to allow dynamic modulation of spatial pooling as a function of the ambient light

level. Interestingly, since presynaptic inhibition was observed in many different sensory systems (Root et al., 2008; Olsen and Wilson, 2008; Baylor et al., 1971; Toyoda and Fujimoto, 1983; Kaneko and Tachibana, 1986; Fahey and Burkhardt, 2003; Kennedy et al., 1974; Burrows and Matheson, 1994; Blagburn and Sattelle, 1987), this mechanism appears general.

Lateral and Feedback GABAergic Circuitry Tunes the L2 Pathway for Processing Dark Object Motion

In addition to mediating surround responses, GABAergic inputs also shape center responses in L2. Blockade of both $GABA_B$Rs on photoreceptors and $GABA_A$Rs distal in the circuit decreases the amplitude of depolarizing responses to decrements and enhances hyperpolarizing responses to increments while making the decrement responses more sustained and hyperpolarizing responses more transient. Since picrotoxin was used to block $GABA_A$Rs, other picrotoxin-sensitive receptors associated with Cl^- channels, such as ionotropic glutamate receptors (Cleland, 1996), could also contribute. These roles of GABA are consistent with previous electrophysiological studies demonstrating GABA-induced depolarizations in LMCs (Hardie, 1987). In addition, receptors distinct from histamine-gated Cl^- channels were previously suggested to contribute to mediating OFF responses in LMCs (Laughlin and Osorio, 1989; Weckström et al., 1989; Juusola et al., 1995).

Previous work demonstrated that calcium signals in L2 cells follow both the depolarizing and hyperpolarizing changes in membrane potential evoked by light (Clark et al., 2011; Dubs, 1982; Laughlin et al., 1987). Here we show that GABAergic signaling is critical to achieving this response property, as its blockade disrupted the near linearity of L2 responses to sinusoidal contrast modulations. Thus, linearity requires regulatory inputs that counteract the otherwise nonlinear responses of L2 that would intrinsically favor hyperpolarizing responses to light ON over depolarizing responses to light OFF. L2 axon terminals were previously described as half-wave rectified (Reiff et al., 2010). However, the variability in response shapes that we describe as emerging from differential filling of center and surround regions may account for much of the discrepancy in the literature (Figures S1B–S1E; Reiff et al., 2010; Clark et al., 2011). Importantly, in the absence of GABAergic circuit inputs, depolarizing responses to decrements are nearly eliminated. Thus, these circuits are required for decrement information to be transmitted to the downstream circuitry and enable its specialization for the detection of moving dark objects. Accordingly, rather than being defined solely by the functional properties of the receptors for photoreceptor outputs, lateral and feedback circuit effects mediated through GABA receptors establish critical aspects of L2 responses.

Distinct Molecular Mechanisms Give Rise to a Similar Early Visual Processing Strategy in Flies and Vertebrates

Early visual processing circuits in flies and vertebrates are thought to be structurally similar (Cajal and Sanchez, 1915; Sanes and Zipursky, 2010). In this parallel, LMCs like L2 are analogous to bipolar cells in the vertebrate retina. Previous work demonstrated that both cell types have antagonistic center-surround RFs (Kaneko, 1970; Järvilehto and Zettler, 1973; Davis and Naka, 1980; Dubs, 1982). However, our detailed characterization of L2 reveals that the functional parallel between these cells is much more significant. First, in both cell types, spatiotemporal coupling arises from delayed surround effects (Figures 3 and 4; Werblin and Dowling, 1969; Laughlin, 1974b; Laughlin and Osorio, 1989; Molnar and Werblin, 2007; Baccus et al., 2008). Second, in both cell types, GABAergic circuitry shapes responses via multiple pathways and affects both response amplitudes and kinetics (Figures 6, 7, and 8; Owen and Hare, 1989; Dong and Werblin, 1998; Euler and Masland, 2000; Shields et al., 2000; Vigh et al., 2011). Interestingly, a differential distribution of GABAergic circuit inputs and receptor types in bipolar cells contributes to heterogeneous responses (Fahey and Burkhardt, 2003; Zhang and Wu, 2009). We hypothesize that different weightings of the same circuit elements that shape L2 responses also differentially shape other LMC responses to tune their function toward distinct downstream processing pathways.

In spite of these deep similarities, many of the molecular mechanisms that shape first-order interneuron responses are different between flies and vertebrates. In OFF bipolar cells, ionotropic glutamate receptors create a sign-conserving synapse with photoreceptors, while metabotropic receptors mediate sign-inverting responses in ON bipolar cells (Masu et al., 1995; Nakanishi et al., 1998; DeVries, 2000). However, in L2 cells, the OFF response is mediated not only by the histamine binding Cl^- channel that mediates photoreceptor outputs but also by GABAergic circuits. Moreover, several mechanisms have been suggested to give rise to surround responses in bipolar cells, including presynaptic inhibition acting on photoreceptors, an ephaptic effect, as well as proton modulation of neurotransmitter release (reviewed in Thoreson and Mangel, 2012). In LMCs, both presynaptic inhibition and extracellular changes in electrical potential have been proposed to mediate spatial and temporal inhibition (Laughlin, 1974a; Shaw, 1975; Laughlin and Hardie, 1978; Hardie, 1987; Laughlin and Osorio, 1989; Juusola et al., 1995; Weckström and Laughlin, 2010). In L2 cells, we found that presynaptic inhibition acting on photoreceptors contributes to surround responses, and $GABA_A$Rs further away from the photoreceptor-LMC synapse are also required (Figures 6, S6, 8, and S7). However, even strong blockade of all GABAergic receptor activity did not completely eliminate the surround, suggesting that additional mechanisms, such as ephaptic effects or other synaptic mechanisms, are also involved.

Overall, the striking similarities between the functional properties of early visual processing circuits across taxa highlight the importance of these properties for efficient processing of visual information. Since these functional properties arise from different molecular mechanisms in flies and vertebrates, these similarities seem unlikely to result from a common ancestral source. Rather, we propose that these parallels reflect convergence on a common processing strategy driven by similar biological constraints and natural input statistics. We speculate that analogous parallels will be found in many other aspects of visual processing.

EXPERIMENTAL PROCEDURES

The Gal4 drivers *21D-Gal4* (Rister et al., 2007) and *Rh1-Gal4* (Bloomington *Drosophila* Stock Center) were used to express a multicopy insert of *UAS-TN-XXL* (Mank et al., 2008; as in Clark et al., 2011) and $GABA_AR$ and $GABA_BR$ RNAis (*$GABA_AR$-RNAi* from VDRC [KK100429] and *$GABA_BR2$-RNAi* from Root et al., 2008). Two-photon imaging was performed using a Leica TSC SP5 II microscope (Leica) equipped with a precompensated Chameleon femtosecond laser (Coherent). Triggering functions provided by the LAS AF Live Data Mode software (Leica) enabled simultaneous initialization and temporal alignment of imaging and visual stimulation. Visual stimulation was applied as described in Clark et al. (2011), except that the stimulus was passed through a 40-nm-wide band-pass spectral filter centered around 562 nm and projected on a back-projection screen situated in front of the fly. All data were acquired at a frame rate of 10.6 Hz. Imaging experiments lasted no more than 2 hr per fly.

SUPPLEMENTAL INFORMATION

Supplemental Information includes seven figures, Supplemental Experimental Procedures, and three tables and can be found with this article online at http://dx.doi.org/10.1016/j.neuron.2013.04.024.

ACKNOWLEDGMENTS

The authors would like to thank Stephen Baccus, Saskia DeVries, Daryl Gohl, Marion Silles, Tina Schwab, Jennifer Esch, and Helen Yang for helpful comments on the manuscript. We would also like to thank Daryl Gohl and Xiaojing Gao (Luo laboratory) for providing fly stocks. This work was supported by a Fulbright Science and Technology Fellowship and a Bio-X Bruce and Elizabeth Dunlevie Stanford Interdisciplinary Graduate Fellowship (L.F.), a Jane Coffin Child's Postdoctoral fellowship (D.A.C.), and a NIH Director's Pioneer Award DP1 OD003530 (T.R.C.) and NIH R01EY022638 (T.R.C.).

Accepted: March 28, 2013
Published: June 19, 2013

REFERENCES

Arnett, D.W. (1972). Spatial and temporal integration properties of units in first optic ganglion of dipterans. J. Neurophysiol. *35*, 429–444.

Atick, J.J. (1992). Could information theory provide an ecological theory of sensory processing? Network *3*, 213–251.

Baccus, S.A., Ölveczky, B.P., Manu, M., and Meister, M. (2008). A retinal circuit that computes object motion. J. Neurosci. *28*, 6807–6817.

Barlow, H. (1961). Possible principles underlying the transformations of sensory messages. In Sensory Communication, W.A. Rosenblith, ed. (Cambridge: MIT Press), pp. 217–234.

Barlow, R.B., Jr. (1969). Inhibitory fields in the Limulus lateral eye. J. Gen. Physiol. *54*, 383–396.

Baylor, D.A., Fuortes, M.G.F., and O'Bryan, P.M. (1971). Receptive fields of cones in the retina of the turtle. J. Physiol. *214*, 265–294.

Blagburn, J.M., and Sattelle, D.B. (1987). Presynaptic depolarization mediates presynaptic inhibition at a synapse between an identified mechanosensory neurone and giant interneurone 3 in the first instar cockroach, periplaneta americana. J. Exp. Biol. *127*, 135–157.

Borst, A., Reisenman, C., and Haag, J. (2003). Adaptation of response transients in fly motion vision. II: Model studies. Vision Res. *43*, 1309–1322.

Borst, A., Haag, J., and Reiff, D.F. (2010). Fly motion vision. Annu. Rev. Neurosci. *33*, 49–70.

Brumberg, J.C., Pinto, D.J., and Simons, D.J. (1996). Spatial gradients and inhibitory summation in the rat whisker barrel system. J. Neurophysiol. *76*, 130–140.

Buchner, E., Bader, R., Buchner, S., Cox, J., Emson, P.C., Flory, E., Heizmann, C.W., Hemm, S., Hofbauer, A., and Oertel, W.H. (1988). Cell-specific immunoprobes for the brain of normal and mutant Drosophila melanogaster. I. Wildtype visual system. Cell Tissue Res. *253*, 357–370.

Burrows, M., and Matheson, T. (1994). A presynaptic gain control mechanism among sensory neurons of a locust leg proprioceptor. J. Neurosci. *14*, 272–282.

Cajal, S.R., and Sanchez, D. (1915). Contribucion al conocimiento de los centros nerviosos del los insectos. Trab. Lab. Invest. Biol. *13*, 1–168.

Clandinin, T.R., and Zipursky, S.L. (2002). Making connections in the fly visual system. Neuron *35*, 827–841.

Clark, D.A., Bursztyn, L., Horowitz, M.A., Schnitzer, M.J., and Clandinin, T.R. (2011). Defining the computational structure of the motion detector in Drosophila. Neuron *70*, 1165–1177.

Cleland, T.A. (1996). Inhibitory glutamate receptor channels. Mol. Neurobiol. *13*, 97–136.

Dacey, D., Packer, O.S., Diller, L., Brainard, D., Peterson, B., and Lee, B. (2000). Center surround receptive field structure of cone bipolar cells in primate retina. Vision Res. *40*, 1801–1811.

Davis, G.W., and Naka, K.-I. (1980). Spatial organization of catfish retinal neurons. I. Single- and random-bar stimulation. J. Neurophysiol. *43*, 807–831.

DeVries, S.H. (2000). Bipolar cells use kainate and AMPA receptors to filter visual information into separate channels. Neuron *28*, 847–856.

Dong, C.-J., and Werblin, F.S. (1998). Temporal contrast enhancement via $GABA_C$ feedback at bipolar terminals in the tiger salamander retina. J. Neurophysiol. *79*, 2171–2180.

Dubs, A. (1982). The spatial integration of signals in the retina and lamina of the fly compound eye under different conditions of luminance. J. Comp. Physiol. A Neuroethol. Sens. Neural Behav. Physiol. *146*, 321–343.

Dubs, A., Laughlin, S.B., and Srinivasan, M.V. (1981). Single photon signals in fly photoreceptors and first order interneurones at behavioral threshold. J. Physiol. *317*, 317–334.

Egelhaaf, M., and Borst, A. (1989). Transient and steady-state response properties of movement detectors. J. Opt. Soc. Am. A *6*, 116–127.

Egelhaaf, M., and Borst, A. (1992). Are there separate ON and OFF channels in fly motion vision? Vis. Neurosci. *8*, 151–164.

Eichner, H., Joesch, M., Schnell, B., Reiff, D.F., and Borst, A. (2011). Internal structure of the fly elementary motion detector. Neuron *70*, 1155–1164.

Enell, L., Hamasaka, Y., Kolodziejczyk, A., and Nässel, D.R. (2007). γ-Aminobutyric acid (GABA) signaling components in Drosophila: immunocytochemical localization of GABA(B) receptors in relation to the GABA(A) receptor subunit RDL and a vesicular GABA transporter. J. Comp. Neurol. *505*, 18–31.

Enroth-Cugell, C., and Freeman, A.W. (1987). The receptive-field spatial structure of cat retinal Y cells. J. Physiol. *384*, 49–79.

Euler, T., and Masland, R.H. (2000). Light-evoked responses of bipolar cells in a mammalian retina. J. Neurophysiol. *83*, 1817–1829.

Fahey, P.K., and Burkhardt, D.A. (2003). Center-surround organization in bipolar cells: symmetry for opposing contrasts. Vis. Neurosci. *20*, 1–10.

Fleet, D.J., and Jepson, A.D. (1985). Spatiotemporal inseparability in early vision: centre-surround models and velocity selectivity. Comput. Intell. *1*, 89–102.

Fleet, D.J., Hallett, P.E., and Jepson, A.D. (1985). Spatiotemporal inseparability in early visual processing. Biol. Cybern. *52*, 153–164.

Glantz, R.M., and Bartels, A. (1994). The spatiotemporal transfer function of crayfish lamina monopolar neurons. J. Neurophysiol. *71*, 2168–2182.

Gollisch, T., and Meister, M. (2010). Eye smarter than scientists believed: neural computations in circuits of the retina. Neuron *65*, 150–164.

Hardie, R.C. (1987). Is histamine a neurotransmitter in insect photoreceptors? J. Comp. Physiol. A Neuroethol. Sens. Neural Behav. Physiol. *161*, 201–213.

Hardie, R.C. (1989). A histamine-activated chloride channel involved in neurotransmission at a photoreceptor synapse. Nature *339*, 704–706.

Hartline, H.K., Wagner, H.G., and Ratliff, F. (1956). Inhibition in the eye of Limulus. J. Gen. Physiol. *39*, 651–673.

Hassenstein, B., and Reichardt, W. (1956). Systemtheoretische analyse der Zeit-, Reihenfolgen- und Vorzeichenauswertung bei der bewegungsperzeption des rüsselkäfers Chlorophanus. Z. Naturforsch. B *11b*, 513–524.

Järvilehto, M., and Zettler, F. (1973). Electrophysiological-histological studies on some functional properties of visual cells and second order neurons of an insect retina. Z. Zellforsch. Mikrosk. Anat.Mikrosk Anat. *136*, 291–306.

Joesch, M., Schnell, B., Raghu, S.V., Reiff, D.F., and Borst, A. (2010). ON and OFF pathways in Drosophila motion vision. Nature *468*, 300–304.

Johnston, D., and Wachtel, H. (1976). Electrophysiological basis for the spatial dependence of the inhibitory coupling in the Limulus retina. J. Gen. Physiol. *67*, 1–25.

Juusola, M., and French, A.S. (1997). Visual acuity for moving objects in first- and second-order neurons of the fly compound eye. J. Neurophysiol. *77*, 1487–1495.

Juusola, M., Weckström, M., Uusitalo, R.O., Korenberg, M.J., and French, A.S. (1995). Nonlinear models of the first synapse in the light-adapted fly retina. J. Neurophysiol. *74*, 2538–2547.

Kaneko, A. (1970). Physiological and morphological identification of horizontal, bipolar and amacrine cells in goldfish retina. J. Physiol. *207*, 623–633.

Kaneko, A., and Tachibana, M. (1986). Effects of γ-aminobutyric acid on isolated cone photoreceptors of the turtle retina. J. Physiol. *373*, 443–461.

Kennedy, D., Calabrese, R.L., and Wine, J.J. (1974). Presynaptic inhibition: primary afferent depolarization in crayfish neurons. Science *186*, 451–454.

Knudsen, E.I., and Konishi, M. (1978). Center-surround organization of auditory receptive fields in the owl. Science *202*, 778–780.

Kolodziejczyk, A., Sun, X., Meinertzhagen, I.A., and Nässel, D.R. (2008). Glutamate, GABA and acetylcholine signaling components in the lamina of the Drosophila visual system. PLoS ONE *3*, e2110.

Laughlin, S.B. (1974a). Neural integration in the first optic neuropile of dragonflies. II. Receptor signal interactions in the lamina. J. Comp. Physiol. A Neuroethol. Sens. Neural Behav. Physiol. *92*, 357–375.

Laughlin, S.B. (1974b). Neural integration in the first optic neuropile of dragonflies. III. The transfer of angular information. J. Comp. Physiol. A Neuroethol. Sens. Neural Behav. Physiol. *92*, 377–396.

Laughlin, S.B. (1981). A simple coding procedure enhances a neuron's information capacity. Z. Naturforsch., C, Biosci. *36*, 910–912.

Laughlin, S.B. (1994). Matching coding, circuits, cells, and molecules to signals: general principles of retinal design in the fly's eye. Prog. Retin. Eye Res. *13*, 165–196.

Laughlin, S.B., and Hardie, R.C. (1978). Common strategies for light adaptation in the peripheral visual systems of fly and dragonfly. J. Comp. Physiol. A Neuroethol. Sens. Neural Behav. Physiol. *128*, 319–340.

Laughlin, S.B., and Osorio, D. (1989). Mechanisms for neural signal enhancement in the blowfly compound eye. J. Exp. Biol. *144*, 113–146.

Laughlin, S.B., Howard, J., and Blakeslee, B. (1987). Synaptic limitations to contrast coding in the retina of the blowfly Calliphora. Proc. R. Soc. Lond. B Biol. Sci. *231*, 437–467.

Liu, X., Krause, W.C., and Davis, R.L. (2007). GABAA receptor RDL inhibits Drosophila olfactory associative learning. Neuron *56*, 1090–1102.

Mank, M., Santos, A.F., Direnberger, S., Mrsic-Flogel, T.D., Hofer, S.B., Stein, V., Hendel, T., Reiff, D.F., Levelt, C., Borst, A., et al. (2008). A genetically encoded calcium indicator for chronic in vivo two-photon imaging. Nat. Methods *5*, 805–811.

Masland, R.H. (2001). The fundamental plan of the retina. Nat. Neurosci. *4*, 877–886.

Masu, M., Iwakabe, H., Tagawa, Y., Miyoshi, T., Yamashita, M., Fukuda, Y., Sasaki, H., Hiroi, K., Nakamura, Y., Shigemoto, R., et al. (1995). Specific deficit of the ON response in visual transmission by targeted disruption of the mGluR6 gene. Cell *80*, 757–765.

Meinertzhagen, I.A., and O'Neil, S.D. (1991). Synaptic organization of columnar elements in the lamina of the wild type in Drosophila melanogaster. J. Comp. Neurol. *305*, 232–263.

Mimura, K. (1976). Some spatial properties in the first optic ganglion of the fly. J. Comp. Physiol. A Neuroethol. Sens. Neural Behav. Physiol. *105*, 65–82.

Molnar, A., and Werblin, F.S. (2007). Inhibitory feedback shapes bipolar cell responses in the rabbit retina. J. Neurophysiol. *98*, 3423–3435.

Nakanishi, S., Nakajima, Y., Masu, M., Ueda, Y., Nakahara, K., Watanabe, D., Yamaguchi, S., Kawabata, S., and Okada, M. (1998). Glutamate receptors: brain function and signal transduction. Brain Res. Brain Res. Rev. *26*, 230–235.

Olsen, S.R., and Wilson, R.I. (2008). Lateral presynaptic inhibition mediates gain control in an olfactory circuit. Nature *452*, 956–960.

Olshausen, B.A., and Field, D.J. (1996). Natural image statistics and efficient coding. Network *7*, 333–339.

Owen, W.G., and Hare, W.A. (1989). Signal transfer from photoreceptors to bipolar cells in the retina of the tiger salamander. Neurosci. Res. Suppl. *10*, S77–S87.

Pitkow, X., and Meister, M. (2012). Decorrelation and efficient coding by retinal ganglion cells. Nat. Neurosci. *15*, 628–635.

Ratliff, F., Hartline, H.K., and Miller, W.H. (1963). Spatial and temporal aspects of retinal inhibitory interaction. J. Opt. Soc. Am. *53*, 110–120.

Reiff, D.F., Plett, J., Mank, M., Griesbeck, O., and Borst, A. (2010). Visualizing retinotopic half-wave rectified input to the motion detection circuitry of Drosophila. Nat. Neurosci. *13*, 973–978.

Richter, J., and Ullman, S. (1982). A model for the temporal organization of X- and Y-type receptive fields in the primate retina. Biol. Cybern. *43*, 127–145.

Rister, J., Pauls, D., Schnell, B., Ting, C.-Y., Lee, C.-H., Sinakevitch, I., Morante, J., Strausfeld, N.J., Ito, K., and Heisenberg, M. (2007). Dissection of the peripheral motion channel in the visual system of Drosophila melanogaster. Neuron *56*, 155–170.

Rivera-Alba, M., Vitaladevuni, S.N., Mishchenko, Y., Lu, Z., Takemura, S.Y., Scheffer, L., Meinertzhagen, I.A., Chklovskii, D.B., and de Polavieja, G.G. (2011). Wiring economy and volume exclusion determine neuronal placement in the Drosophila brain. Curr. Biol. *21*, 2000–2005.

Rodieck, R.W. (1965). Quantitative analysis of cat retinal ganglion cell response to visual stimuli. Vision Res. *5*, 583–601.

Root, C.M., Masuyama, K., Green, D.S., Enell, L.E., Nässel, D.R., Lee, C.-H., and Wang, J.W. (2008). A presynaptic gain control mechanism fine-tunes olfactory behavior. Neuron *59*, 311–321.

Sanes, J.R., and Zipursky, S.L. (2010). Design principles of insect and vertebrate visual systems. Neuron *66*, 15–36.

Shapley, R., and Lennie, P. (1985). Spatial frequency analysis in the visual system. Annu. Rev. Neurosci. *8*, 547–583.

Shaw, S.R. (1975). Retinal resistance barriers and electrical lateral inhibition. Nature *255*, 480–482.

Shields, C.R., Tran, M.N., Wong, R.O., and Lukasiewicz, P.D. (2000). Distinct ionotropic GABA receptors mediate presynaptic and postsynaptic inhibition in retinal bipolar cells. J. Neurosci. *20*, 2673–2682.

Srinivasan, M.V. (1990). Generalized gradient schemes for the measurement of two-dimensional image motion. Biol. Cybern. *63*, 421–431.

Srinivasan, M.V., and Dvorak, D.R. (1980). Spatial processing of visual information in the movement-detecting pathway of the fly. J. Comp. Physiol. A Neuroethol. Sens. Neural Behav. Physiol. *140*, 1–23.

Srinivasan, M.V., Laughlin, S.B., and Dubs, A. (1982). Predictive coding: a fresh view of inhibition in the retina. Proc. R. Soc. Lond. B Biol. Sci. *216*, 427–459.

Srinivasan, M.V., Pinter, R.B., and Osorio, D. (1990). Matched filtering in the visual system of the fly: large monopolar cells of the lamina are optimized to detect moving edges and blobs. Proc. R. Soc. Lond. B Biol. Sci. *240*, 279–293.

Stavenga, D.G. (2003). Angular and spectral sensitivity of fly photoreceptors. II. Dependence on facet lens F-number and rhabdomere type in Drosophila. J. Comp. Physiol. A Neuroethol. Sens. Neural Behav. Physiol. *189*, 189–202.

Tammero, L.F., Frye, M.A., and Dickinson, M.H. (2004). Spatial organization of visuomotor reflexes in Drosophila. J. Exp. Biol. *207*, 113–122.

Thoreson, W.B., and Mangel, S.C. (2012). Lateral interactions in the outer retina. Prog. Retin. Eye Res. *31*, 407–441.

Toyoda, J.-I., and Fujimoto, M. (1983). Analyses of neural mechanisms mediating the effect of horizontal cell polarization. Vision Res. *23*, 1143–1150.

van Hateren, J.H. (1992). Theoretical predictions of spatiotemporal receptive fields of fly LMCs, and experimental validation. J. Comp. Physiol. A Neuroethol. Sens. Neural Behav. Physiol. *171*, 157–170.

Vigh, J., Vickers, E., and von Gersdorff, H. (2011). Light-evoked lateral GABAergic inhibition at single bipolar cell synaptic terminals is driven by distinct retinal microcircuits. J. Neurosci. *31*, 15884–15893.

Weber, F., Machens, C.K., and Borst, A. (2010). Spatiotemporal response properties of optic-flow processing neurons. Neuron *67*, 629–642.

Weckström, M., and Laughlin, S. (2010). Extracellular potentials modify the transfer of information at photoreceptor output synapses in the blowfly compound eye. J. Neurosci. *30*, 9557–9566.

Weckström, M., Kouvalainen, E., Djupsund, K., and Järvilehto, M. (1989). More than one type of conductance is activated during responses of Blowfly monopolar neurones. J. Exp. Biol. *144*, 147–154.

Werblin, F.S., and Dowling, J.E. (1969). Organization of the retina of the mudpuppy, Necturus maculosus. II. Intracellular recording. J. Neurophysiol. *32*, 339–355.

Wilson, R.I., and Laurent, G. (2005). Role of GABAergic inhibition in shaping odor-evoked spatiotemporal patterns in the Drosophila antennal lobe. J. Neurosci. *25*, 9069–9079.

Zanker, J.M., Srinivasan, M.V., and Egelhaaf, M. (1999). Speed tuning in elementary motion detectors of the correlation type. Biol. Cybern. *80*, 109–116.

Zhang, A.J., and Wu, S.M. (2009). Receptive fields of retinal bipolar cells are mediated by heterogeneous synaptic circuitry. J. Neurosci. *29*, 789–797.